JOURNAL OF PROPULSION AND POWER
Vol. 20, No. 6, November–December 2004

# Performance of a Jet-Pumped Cryogenic Refrigeration System

S. M. Kandil,* W. E. Lear,† and S. A. Sherif‡
*University of Florida, Gainesville, Florida 32611-6300*

**Efficient, lightweight thermal management and power systems are crucial for successful exploration of space. This paper provides an analysis of a novel solar-integrated thermal management and power system, which is comprised of a thermally actuated heat pump with power and refrigeration subsystems and having a jet pump serving as the compression device. The analysis allows calculation of on an overall system mass ratio that compares the overall active system mass to an idealized passive counterpart. In this study liquid nitrogen, which is common on many space missions, is the working fluid. This achieves a significant mass advantage as the use of cryocoolers is eliminated. By applying the techniques demonstrated in this paper, designers can identify and optimize conceptual configurations during the initial prototype development stages to reduce payload weight and increase financial savings.**

## Nomenclature

| | | |
|---|---|---|
| $A$ | = | cross-sectional area, m$^2$ |
| $a$ | = | speed of sound, m/s |
| $G_{\text{sun}}$ | = | local radiant solar heat flux, W/m$^2$ |
| $h$ | = | specific enthalpy, kJ/kg |
| $M$ | = | Mach number |
| $m$ | = | mass, kg |
| $\tilde{m}$ | = | system mass ratio (SMR) |
| $\dot{m}$ | = | mass flow rate, kg/s |
| $P$ | = | pressure, MPa |
| $P_r$ | = | compression ratio |
| $Q'$ | = | heat transfer rate, kW |
| $r$ | = | heat exchanger pressure ratio |
| $T$ | = | temperature, °C |
| $T^*$ | = | normalized temperature |
| $V$ | = | velocity, m/s |
| $w'$ | = | work rate, kW |
| $\alpha$ | = | mass per unit area ratio |
| $\varepsilon$ | = | emissivity |
| $\zeta$ | = | collector parameter |
| $\eta$ | = | efficiency |
| $\lambda$ | = | mass per unit area, kg/m$^2$ |
| $\mu$ | = | turbomachinery mass fraction |
| $\xi$ | = | percentage of Carnot efficiency |
| $\rho$ | = | density, kg/m$^3$ |
| $\sigma$ | = | Stephan–Boltzmann constant, $5.67 \times 10^{-8}$ W/m$^2$-K$^4$ |
| $\phi$ | = | entrainment ratio, $\dot{m}_s/\dot{m}_p$ |

*Subscripts*

*System mass ratio analysis.*

| | | |
|---|---|---|
| $C$ | = | Carnot |
| col | = | collector |
| $e$ | = | high-temperature reservoir source, refrigeration cycle |
| $H$ | = | high-temperature reservoir source, power cycle |
| $P$ | = | power |
| $R$ | = | refrigeration |
| rad | = | radiator |
| rad, o | = | ideal passive radiator |
| rad, p | = | actual passive radiator |
| SMR | = | system mass ratio |
| $s$ | = | surrounding temperature reservoir source |
| sys | = | system, excluding collector and radiator |
| $T$ | = | total |
| t, act | = | total actual system including collector and radiator |

*SITMAP analysis.*

| | | |
|---|---|---|
| de | = | diffuser exit |
| ei | = | evaporator inlet |
| evap | = | evaporator |
| me | = | mixing chamber exit |
| ne | = | primary nozzle exit |
| nt | = | primary nozzle throat |
| p | = | primary flow |
| pe | = | pump exit |
| pi | = | primary nozzle inlet |
| pump | = | mechanical pump |
| rad | = | radiator |
| re | = | radiator exit |
| $s$ | = | secondary flow |
| sc | = | solar collector |
| se | = | secondary flow exit |
| si | = | secondary flow inlet |
| ss | = | state immediately downstream of shock wave |
| $t$ | = | turbine |
| ti | = | turbine inlet |
| ts | = | isentropic turbine exit state |

Received 30 January 2002; revision received 20 January 2004; accepted for publication 27 January 2004. Copyright © 2004 by the authors. Published by the American Institute of Aeronautics and Astronautics, Inc., with permission. Copies of this paper may be made for personal or internal use, on condition that the copier pay the $10.00 per-copy fee to the Copyright Clearance Center, Inc., 222 Rosewood Drive, Danvers, MA 01923; include the code 0748-4658/04 $10.00 in correspondence with the CCC.

*Research Assistant, Department of Mechanical and Aerospace Engineering, 237 MAE Building, P.O. Box 116300.

†Associate Professor, Department of Mechanical and Aerospace Engineering, 237 MAE Building, P.O. Box 116300. Associate Fellow AIAA.

‡Professor, Department of Mechanical and Aerospace Engineering, 237 MAE Building, P.O. Box 116300; sasherif@ufl.edu. Associate Fellow AIAA.

## Introduction

THE increased interest in space exploration and the importance of a human presence in space are significant driving forces behind space power and thermal management improvements. One of the most important aspects of the desired enhancements is to have lightweight space power-generation capabilities. Onboard power generation adds weight to the space platform not only because of its inherent weight, but also because of the increased weight of the required thermal management systems.

The work presented in this paper is based on the work done by Nord et al.[1] and Freudenberg et al.[2] Nord et al.[1] developed a combined power and thermal management cycle for onboard spacecraft applications. The cycle is referred to as the Solar Integrated Thermal Management and Power cycle (SITMAP), shown in Fig. 1. This cycle is essentially a combined vapor compression cycle and

Rankine cycle with the compression device being a jet pump instead of the regular compressor. The jet pump has several advantages for space applications, as it involves no moving parts, which decreases the weight and vibration level while increasing the reliability. The power subsystem is a Rankine cycle, which drives the system. The jet pump acts as the joining device between the thermal and power subsystems, by mixing the high-pressure flow from the power subsystem with the low-pressure flow from the refrigeration subsystem providing a pressure increase in the refrigeration cycle. Nord et al.[1] used Refrigerant 134-a as the working fluid in their analysis. The mechanical power produced by the turbine can be used to drive the mechanical pump as well as other onboard applications. This allows the SITMAP cycle to be solely driven by solar thermal input. Examples of work relevant to the SITMAP investigation include Bredikhin et al.,[3] Cunningham and Dopkin,[4] Cunningham,[5] Elger et al.,[6] Fabri and Paulon,[7] Fabri and Siestrunk,[8] Fairuzov and Bredikhin,[9] Holladay and Hunt,[10] Holmes et al.,[11] Jiao et al.,[12] Lear et al.,[13] Marini et al.,[14] Neve,[15] and Sherif et al.[16] Literature dealing with thermally actuated cooling systems includes those by Kakabaev and Davletov,[17] Chen,[18] Lansing and Chai,[19] and Chai and Lansing.[20]

Freudenberg et al.,[2] motivated by the novel SITMAP cycle developed by Nord et al.,[1] developed an expression for a system mass ratio (SMR) as a mass-based figure of merit for any thermally actuated heat pump with power and thermal management subsystems. SMR is a ratio between the overall system mass to the mass of an ideal passive radiator, where there is no refrigeration subsystem, in which the ideal radiator operates at the same temperature as the cooling load. SMR depends on several dimensionless parameters including three temperature parameters as well as structural and efficiency parameters. Freudenberg et al.[2] estimated the range of each parameter for a typical thermally actuated cooling system operating in space. They investigated the effect of varying each of the parameters within the estimated range, comparing their analysis to a base model based on the average value of each of the ranges. Many systems dealing with power and thermal management have been proposed for which this analysis can be used, including absorption cooling systems and solar-powered vapor jet refrigeration systems. Examples of these systems are found in the works of Abrahamsson et al.,[21] Alefeld and Radermacher,[22] Anderson,[23] Chai and Lansing,[20] Chen,[18] and Lansing and Chai.[19]

The purpose of this work is to apply the SMR analysis, presented by Freudenberg et al.,[2] to the SITMAP cycle developed by Nord et al.[1] to study the effect of different SITMAP parameters on the overall mass of the system. The inputs to the SITMAP analysis, as presented by Nord et al.,[1] are the inlet states for the jet pump and the entrainment ratio, defined as the ratio between the secondary flow (flow rate in the refrigeration loop) to the primary flow (flow rate in the power loop). For this purpose, seven cases were developed for the SITMAP cycle (summarized in Table 1) with different values of the five SITMAP parameters, with the base case being case 1. As mentioned earlier, the SMR depends on seven dimensionless parameters. Three of the SMR parameters are dictated by the SITMAP cycle analysis; those parameters are the collector temperature $T^*_{\text{col}}$, radiator temperature $T^*_{\text{rad}}$, and the overall percentage Carnot efficiency $\xi_T$. Thus, for each of the seven cases the effect of the remaining SMR parameters on the SMR will be investigated.

In this paper, liquid nitrogen will be used as the working fluid. One particular advantage for the use of liquid nitrogen is its presence onboard for cooling sensors and imaging systems. Thus, its use as the working fluid will allow for self-cooling as an alternative to conventional cryocoolers, adding a further weight advantage for the SITMAP cycle.

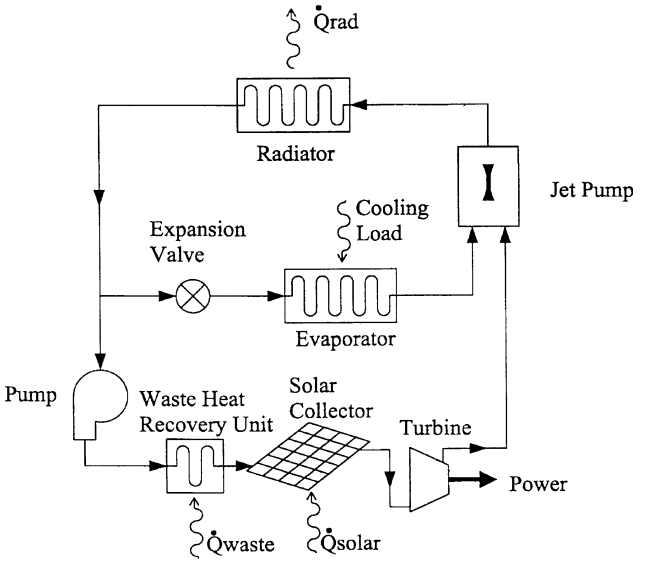


**Fig. 1 Schematic of the SITMAP cycle.**

## Analysis

Nord et al.[1] presented a detailed analysis for the jet pump and the SITMAP cycle, whereas Freudenberg et al.[2] discussed the SMR calculation in detail. Both analyses will be briefly presented in this paper.

### Jet Pump

Figure 2 shows a schematic of the jet pump. The high-pressure primary flow from the power loop (state pi) is expanded in a converging–diverging supersonic nozzle until the pressure matches that of the secondary exit. Constant pressure mixing takes place in the mixing chamber before entering the diffuser. The complete method for calculating the diffuser exit state and the jet pump geometry given the primary and secondary inlet states and the entrainment ratio $\phi$ is shown next.

*Primary Nozzle*

To obtain the properties at the nozzle throat, guess $P_{\text{nt}}$, and estimate that $s_{\text{nt}} = s_{\text{pi}}$. Calculate the primary nozzle inlet velocity using the continuity equation

$$V_{\text{pi}} = (\rho_{\text{nt}}/\rho_{\text{pi}})(A_{\text{nt}}/A_{\text{pi}})V_{\text{nt}} \tag{1}$$

**Table 1 Summary of the inputs and outputs of the SITMAP cycle analysis and values of the SMR parameters dictated by the SITMAP analysis**

| | SITMAP inputs | | | | | SITMAP outputs | | | | SMR parameters | | |
|---|---|---|---|---|---|---|---|---|---|---|---|---|
| Case number | $T_{\text{pi}}$ | $P_{\text{pi}}$ | $T_{\text{si}}$ | $P_{\text{si}}$ | $\phi$ | $P_r$ | $\eta_{\text{th}}$ COP | $Q_{\text{evap}}$ | $Q_{\text{rad}}$ | $T^*_{\text{col}}$ | $T^*_{\text{rad}}$ | $\xi_T$ |
| 1 | −80 | 2 | −175 | 0.4 | 2 | 1.483 | 1.298 | 354.11 | 626.84 | 1.994 | 1.303 | 1.136 |
| 2 | −80 | 8 | −175 | 0.4 | 2 | 1.867 | 1.461 | 339.77 | 572.33 | 2.173 | 1.225 | 0.754 |
| 3 | −80 | 2 | −110 | 1.4 | 2 | 1.106 | 1.741 | 412.92 | 650.14 | 1.191 | 1.060 | 0.948 |
| 4 | 40 | 2 | −175 | 0.4 | 2 | 1.544 | 0.873 | 351.53 | 754.39 | 3.214 | 1.709 | 1.320 |
| 5 | 40 | 2 | −20 | 0.4 | 2 | 1.376 | 1.706 | 693.52 | 1099.95 | 1.246 | 1.077 | 0.957 |
| 6 | −80 | 2 | −175 | 0.4 | 0.2 | 3.725 | 0.120 | 28.67 | 267.69 | 1.981 | 1.799 | 1.040 |
| 7 | −80 | 2 | −175 | 0.4 | 6 | 1.089 | 3.959 | 1113.48 | 1394.74 | 1.996 | 1.122 | 1.106 |
| 8 | −80 | 2 | −164 | 1.4 | 2 | 1.210 | 0.520 | 120.96 | 353.47 | 1.778 | 1.031 | 0.039 |

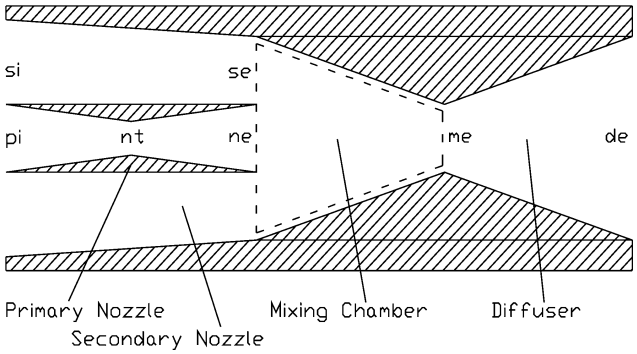


**Fig. 2 Jet pump schematic: – – –, control volume used for the momentum analysis.**

Calculate the velocity at the nozzle throat using conservation of energy

$$V_{nt} = \left( \frac{h_{pi} - h_{nt}}{\frac{1}{2}\left\{1 - [(\rho_{nt}/\rho_{pi})(A_{nt}/A_{pi})]^2\right\}} \right)^{\frac{1}{2}} \tag{2}$$

Calculate the Mach number at the nozzle throat using Eqs. (3) and (4). The $s$ in Eq. (3) signifies an isentropic process

$$a = \sqrt{\left(\frac{\partial P}{\partial \rho}\right)_s} \tag{3}$$

$$M = \frac{V}{a} \tag{4}$$

Iterate (change $P_{nt}$) until the Mach number is equal to unity.

To obtain the properties at the nozzle exit, estimate that $s_{ne} = s_{nt}$, and assert that $P_{ne} = P_{se}$. For the current analysis, $P_{se}/P_{si} = 0.95$ was specified. (This yields a secondary exit velocity of 45 m/s when state si is the stagnation state). Calculate the primary nozzle-exit velocity using conservation of energy

$$V_{ne} = \left[2\left(h_{nt} + \tfrac{1}{2}V_{nt}^2 - h_{ne}\right)\right]^{\frac{1}{2}} \tag{5}$$

Calculate the ratio $A_{nt}/A_{ne}$ using the continuity equation

$$A_{nt}/A_{ne} = (\rho_{ne}/\rho_{nt})(V_{ne}/V_{nt}) \tag{6}$$

Calculate the Mach number at the primary nozzle exit using Eqs. (3) and (4).

*Secondary Flow*

Specify $A_{se}/A_{si}$ and guess $A_{ne}/A_{se}$. Estimate that $s_{se} = s_{si}$, and calculate the velocity at the secondary inlet using the continuity equation and the definition of the entrainment ratio (Note: $P_{se}$ has been previously specified):

$$V_{si} = \phi(\rho_{ne}/\rho_{si})(A_{ne}/A_{se})(A_{se}/A_{si})V_{ne} \tag{7}$$

Calculate the velocity at the secondary exit using conservation of energy and Eq. (7):

$$V_{se} = \left[2\left(h_{si} + \tfrac{1}{2}V_{si}^2 - h_{se}\right)\right]^{\frac{1}{2}} \tag{8}$$

Calculate the area ratio $A_{ne}/A_{se}$ using the continuity equation and the definition of the entrainment ratio

$$A_{ne}/A_{se} = (1/\phi)(\rho_{se}/\rho_{ne})(V_{se}/V_{ne}) \tag{9}$$

Iterate on $A_{ne}/A_{se}$. Calculate the Mach number at the secondary exit using Eqs. (3) and (4).

*Mixing Chamber*

Calculate the velocity at the mixing chamber exit using the continuity equation and the integral form of the momentum equation. The geometry of the mixing chamber is defined such that the mixing process occurs at constant pressure. Defining the control volume as shown in Fig. 2, the momentum equation, Eq. (10), can be combined with Eq. (11) and the definition of the entrainment ratio to obtain Eq. (12), the mixing chamber exit velocity

$$(P_{ne} - P_{se})A_{ne} = -\dot{m}_p V_{ne} - \phi\dot{m}_p V_{se} + (1+\phi)\dot{m}_p V_{me} \tag{10}$$

$$\dot{m}_p = \rho_{ne} A_{ne} V_{ne} \tag{11}$$

$$V_{me} = \frac{P_{ne} - P_{se} + \rho_{ne}V_{ne}^2[1 + \phi(V_{se}/V_{ne})]}{(1+\phi)\rho_{ne}V_{ne}} \tag{12}$$

Calculate the mixing chamber exit specific enthalpy and the area ratio $A_{me}/A_{ne}$ using conservation of energy and the continuity equation, respectively:

$$h_{me} = [1/(1+\phi)]\left[h_{ne} + \tfrac{1}{2}V_{ne}^2 + \phi\left(h_{se} + \tfrac{1}{2}V_{se}^2\right)\right] - \tfrac{1}{2}V_{me}^2 \tag{13}$$

$$A_{me}/A_{ne} = (1+\phi)(\rho_{ne}/\rho_{me})(V_{ne}/V_{me}) \tag{14}$$

Calculate the mixing chamber exit Mach number using Eqs. (3) and (4).

*Diffuser*

It is possible that the mixing chamber exit flow is supersonic. In such a case, a shock exists in the diffuser. This analysis assumes that the shock occurs at the diffuser inlet where the Mach number is closest to unity, and, thus, the stagnation pressure loss over the shock is minimized.

If $M_{me} > 1$, guess $P_{ss}$, and assume Eqs. (15–18) apply for the shock

$$\rho_{me}V_{me} = \rho_{ss}V_{ss} \tag{15}$$

$$P_{me} + \rho_{me}V_{me}^2 = P_{ss} + \rho_{ss}V_{ss}^2 \tag{16}$$

$$h_{me} + \tfrac{1}{2}V_{me}^2 = h_{ss} + \tfrac{1}{2}V_{ss}^2 \tag{17}$$

$$\rho_{ss} = \rho(P_{ss}, h_{ss}) \tag{18}$$

Equations (15) and (16) can be combined to obtain the velocity downstream of the shock.

$$V_{ss} = \frac{P_{me} + \rho_{me}V_{me}^2 - P_{ss}}{\rho_{me}V_{me}} \tag{19}$$

Equation (19) can be combined with Eq. (15) to obtain the density downstream of the shock. Equation (19) can also be used with Eq. (17) to obtain the specific enthalpy downstream of the shock, which can be used with Eq. (18) to obtain the density downstream of the shock. Iterate on $P_{ss}$ until the density obtained from Eq. (15) matches that from Eq. (18). To obtain the diffuser exit state for the case of $M_{me} > 1$, follow the procedure for $M_{me}$ less than or equal to 1, replacing the subscript me with ss.

If $M_{me}$ is less than or equal to 1, then to obtain the properties at the diffuser exit guess $P_{de}$, and use the estimation that $s_{de} = s_{me}$. Calculate the velocity at the diffuser exit using the continuity equation

$$V_{de} = (\rho_{me}/\rho_{de})(A_{me}/A_{ne})(A_{ne}/A_{de})V_{me} \tag{20}$$

Calculate the velocity at the diffuser exit using conservation of energy

$$V_{de} = \left[2\left(h_{me} + \tfrac{1}{2}V_{me}^2 - h_{de}\right)\right]^{\frac{1}{2}} \tag{21}$$

Iterate (change $P_{de}$) until the continuity equation and conservation of energy yield the same diffuser exit velocity. Calculate the Mach number at the diffuser exit using Eqs. (3) and (4).

The preceding jet pump analysis is general and applies to all flow regimes, including two-phase flow. The results can be used in the following SITMAP cycle analysis.

**SITMAP Cycle**

Figure 2 shows the SITMAP cycle. The method used to achieve a converged solution for the SITMAP cycle given the jet pump inlet and exit states and entrainment ratio follows. The solar collector efficiency was estimated at 80%, and the pump, turbine, and radiator efficiencies were estimated to be 95%. Frictional pressure losses in the system were lumped into an estimated pressure ratio over the various heat exchangers of $r = 0.97$. The jet pump primary inlet corresponds to the turbine exit state.

*Overall Analysis*

System convergence requires a double-iterative solution. The first step requires guessing the turbine inlet state ($P_{ti}$ and $T_{ti}$), the specific enthalpy from Eq. (22), and the fact that $P_{ts} = P_{pi}$ can then be used to calculate an isentropic turbine exit state. From the definition of turbine efficiency,

$$h_{ts} = h_{ti} - (h_{ti} - h_{pi})/\eta_t \tag{22}$$

Iterate on $T_{ti}$ until the entropy corresponding to the current turbine inlet state matches that of the calculated isentropic turbine exit state.

At this point, the correct inlet temperature corresponding to the guessed turbine inlet pressure and the specified turbine efficiency has been obtained. The next step is to invoke the work balance between the pump and turbine and use the heat-exchanger pressure ratio to determine the validity of the guessed turbine inlet pressure

$$\dot{W}_t = \dot{m}_p(h_{ti} - h_{pi}) \tag{23}$$

$$\dot{W}_{pump} = (\dot{m}_p/\eta_{pump}\rho_{re})(P_{pe} - P_{re}) \tag{24}$$

$$P_{pe} = P_{re} + \dot{W}_{pump}\eta_{pump}\rho_{re}/\dot{m}_p \tag{25}$$

$$P_{ti} = P_{pe}r^2 \tag{26}$$

Iterate on $P_{ti}$ (repeat the entire SITMAP analysis) until it matches that obtained by Eq. (26).

A converged solution has now been obtained for the SITMAP cycle. The following equations complete the analysis:

$$h_{pe} = h_{re} + (h_{ti} - h_{pi}) \tag{27}$$

$$h_{ei} = h_{re} \tag{28}$$

$$\dot{Q}_{evap} = \phi\dot{m}_p(h_{si} - h_{ei}) \tag{29}$$

$$\dot{Q}_{rad} = \dot{m}_p(1 + \phi)(h_{de} - h_{re}) \tag{30}$$

$$\dot{Q}_{sc} = \dot{m}_p(h_{ti} - h_{pe}) \tag{31}$$

Note that Eq. (31) assumes the worst-case scenario of no waste heat recovery.

*Solar-Collector Model*

The solar collector was modeled using a solar constant of $G_{sun} = 1353$ W/m$^2$. Generally, $G_{sun}$ varies with the distance from the sun. Equation (32) was used to estimate the area of the solar collector

$$A_{sc} = \dot{Q}_{sc}/\eta_{sc}G_{sun} \tag{32}$$

*Radiator Model*

Equation (33) represents the energy balance between the fluid and the radiator; the emissivity has been lumped into an overall radiator efficiency $\eta_{rad}$,

$$dA_{rad} = (-\dot{m}_p/\eta_{rad}\sigma)T_{rad}^{-4}\,dh_{rad} \tag{33}$$

If superheat exists at the radiator inlet, Eq. (33) must be numerically integrated to account for decreasing temperature in the superheated region. For saturated flow, Eq. (33) can be analytically integrated, using the estimation of constant temperature at an average saturation pressure over the radiator.

To efficiently perform the preceding calculations and create performance graphs, a program called JetSit was developed by Nord et al.[1] JetSit's main functions are to calculate the jet pump geometry and diffuser exit state and to use those results to calculate a solution to the SITMAP cycle. JetSit is able to analyze jet pump solutions for all flow regimes, including saturated flow. To perform the analysis in this paper, modifications were made to the JetSit code to be able to change the working fluid to nitrogen and incorporate wider working fluid state regimes.

**System Mass Ratio**

Figure 3 shows a schematic for the conceptual thermally actuated heat pump system being considered. The power subsystem accepts heat from a high-temperature source and supplies the power needed by the refrigeration subsystem. Both systems reject heat via a radiator to a common heat sink. The power cycle supplies just enough power internally to maintain and operate the refrigeration loop. However, in principle, the power cycle could provide power for other onboard systems if needed. Both the power and refrigeration systems are considered generic and can be modeled by any specific type of heat engine such as the Rankine, Sterling, and Brayton cycles for the power subsystem and gas refrigeration or vapor compression cycles for the cooling subsystem.

The SMR is defined as the ratio between the mass of the overall system and that of an idealized passive system. The overall system mass is divided into three terms: radiator, collector, and a general system mass comprising the turbomachinery and piping present in an active system. This is shown mathematically by

$$\tilde{m} = (m_{col} + m_{rad} + m_{sys})/m_{rad,o} \tag{34}$$

Equation (34) can be separated and rewritten in terms of collector and radiator areas

$$\tilde{m} = \frac{(\lambda_{col}/\lambda_{rad})A_{col} + A_{rad}}{A_{rad,o}} + \frac{m_{sys}}{m_{rad,o}} \tag{35}$$

The solar collector was modeled by examining the solar energy incident on its surface. This energy is proportional to the collector efficiency, the cross-sectional area that is absorbing the flux, and the local radiant solar heat flux $G_{sun}$, same as Eq. (32).

The radiant energy transfer rate between the radiator and the environment is given next. For deep-space applications, the environmental reservoir temperature can be neglected, but for near-planetary or solar missions this might not be the case.

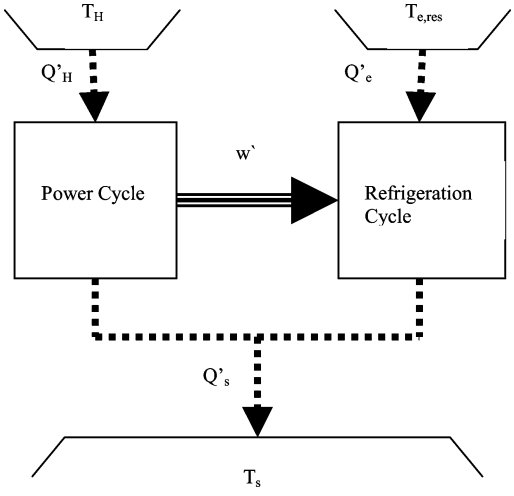


**Fig. 3 Overall system schematic for SMR analysis.**

$$Q'_s = \varepsilon\sigma A_{\text{rad}}\left(T_{\text{rad}}^4 - T_s^4\right) \tag{36}$$

The idealized passive radiator model operates perfectly ($\varepsilon = 1$) at the temperature of the evaporator, that is, the load temperature. Because there is no additional thermal input, the heat transferred to the radiator is equal to that transferred from the evaporator. The ideal passive area for a radiator is consistent with

$$Q'_{\text{passive}} = \sigma A_{\text{rad,o}}\left(T_e^4 - T_s^4\right) = Q'_e \tag{37}$$

Defining a new nondimensional parameter $\alpha$ as $\alpha = \lambda_{\text{col}}/\lambda_{\text{rad}}$, performing an overall energy balance on the active system yielding $Q'_H + Q'_e = Q'_s$, and substituting Eqs. (32), (36), and (37) into Eq. (35) yields

$$\tilde{m} = \frac{1}{\varepsilon}\left(\frac{Q'_H}{Q'_e}\left[1 - \left(\frac{T_s}{T_e}\right)^4\right]\left\{\frac{\alpha\varepsilon\sigma T_e^4}{\eta_{\text{col}} G_{\text{sun}}} + \left(\frac{T_e}{T_{\text{rad}}}\right)^4\left[\frac{1}{1-(T_s/T_{\text{rad}})^4}\right]\right\} + \left(\frac{T_e}{T_{\text{rad}}}\right)^4\left[\frac{1-(T_s/T_e)^4}{1-(T_s/T_{\text{rad}})^4}\right]\right) + \frac{m_{\text{sys}}}{m_{\text{rad,o}}} \tag{38}$$

Substituting the following definitions

$$\eta = w'/Q'_H, \qquad COP = Q'_e/w'$$

$$\eta COP = Q'_e/Q'_H \tag{39}$$

$$\xi_P = \eta/\eta_C, \qquad \xi_R = COP/COP_C, \qquad \xi_T = \xi_P\xi_R \tag{40}$$

$$\eta_C = 1 - T_{\text{rad}}/T_{\text{col}}, \qquad COP_C = T_e/(T_{\text{rad}} - T_e)$$

$$\zeta = \alpha\varepsilon\sigma T_e^4/\eta_{\text{col}} G_{\text{sun}} \tag{41}$$

$$T^*_{\text{col}} = T_{\text{col}}/T_e, \qquad T^*_{\text{rad}} = T_{\text{rad}}/T_e, \qquad T^*_s = T_s/T_e \tag{42}$$

into Eq. (38) yields

$$\tilde{m} = \frac{1}{\varepsilon}\left\{\frac{T^*_{\text{col}}\left(T^*_{\text{rad}} - 1\right)\left(1 - T^{*4}_s\right)}{\xi_T\left(T^*_{\text{col}} - T^*_{\text{rad}}\right)}\left[\zeta + \left(\frac{1}{T^{*4}_{\text{rad}} - T^{*4}_s}\right)\right] + \left(\frac{1 - T^{*4}_s}{T^{*4}_{\text{rad}} - T^{*4}_s}\right)\right\} + \frac{m_{\text{sys}}}{m_{\text{rad,o}}} \tag{43}$$

Nondimensionalizing to the third term on the right-hand side of Eq. (43) yields

$$(m_{\text{sys}}/m_{t,\text{act}})(m_{t,\text{act}}/m_{\text{rad,o}}) = (m_{\text{sys}}/m_{t,\text{act}})\tilde{m} \tag{44}$$

But $m_{t,\text{act}} = m_{\text{rad}} + m_{\text{col}} + m_{\text{sys}}$; therefore,

$$\tilde{m} = \frac{1}{\varepsilon}\left\{\frac{T^*_{\text{col}}\left(T^*_{\text{rad}} - 1\right)\left(1 - T^{*4}_s\right)}{\xi_T\left(T^*_{\text{col}} - T^*_{\text{rad}}\right)}\left[\zeta + \left(\frac{1}{T^{*4}_{\text{rad}} - T^{*4}_s}\right)\right] + \left(\frac{1 - T^{*4}_s}{T^{*4}_{\text{rad}} - T^{*4}_s}\right)\right\} + \frac{m_{\text{sys}}}{m_{t,\text{act}}}\tilde{m} \tag{45}$$

Defining $\mu = m_{\text{sys}}/m_{t,\text{act}}$ yields

$$\tilde{m} = \frac{1}{\varepsilon(1-\mu)}\left\{\frac{T^*_{\text{col}}\left(T^*_{\text{rad}} - 1\right)\left(1 - T^{*4}_s\right)}{\xi_T\left(T^*_{\text{col}} - T^*_{\text{rad}}\right)} \times\left[\zeta + \left(\frac{1}{T^{*4}_{\text{rad}} - T^{*4}_s}\right)\right] + \left(\frac{1 - T^{*4}_s}{T^{*4}_{\text{rad}} - T^{*4}_s}\right)\right\} \tag{46}$$

Equation (46) represents the SMR in terms of seven system parameters. Three of these parameters are based on temperature ratios, and the remaining four are based on system properties. All of the parameters are quantities that can be computed for a given application.

## Results and Discussion

As mentioned earlier, three of the seven dimensionless parameters are dictated by the SITMAP cycle analysis. Those three variables are listed in the last three columns of Table 1, for each of the eight cases cited in the table. Two of the remaining four parameters will be fixed for all of the eight cases because their effect is predicted, and thus not of interest for parametric investigation. Those parameters are the emissivity $\varepsilon$ and the mass ratio $\mu$. The emissivity $\varepsilon$ will be held constant at 0.865, and $\mu$ at 0.5 as suggested by Freudenberg et al.[2] The effect of the remaining two parameters, namely, the normalized sink temperature $T^*_s$ and the collector parameter $\zeta$, is investigated by considering them to be the independent variables in the analysis.

The effect of the five SITMAP input parameters is studied through performing the SMR analysis on the eight cases shown in Table 1. Case 1 is the base case for comparison. For each of the other seven cases, the effect of individual parameters is demonstrated by changing its value while maintaining all other parameters at their base value.

Before discussing the effect of individual parameters, it should be noted that there are two general trends in Fig. 4–11. First, the SMR value increases with increasing values of the collector parameter $\zeta$. This can be explained by examining Eq. (41) for $\zeta$. It can be seen that increasing $\zeta$ implies one of several effects, such as the increase of the mass per unit area of the collector and radiator, the increase of the cooling load temperature, or the decrease in the collector efficiency. All of those effects naturally result in increasing the overall system mass. Clearly, lightweight heat exchangers and low evaporator temperatures favor active systems. The second general trend in all figures is the apparent decrease of the SMR with increasing the normalized environment (sink) temperature. This effect is apparent because increasing the environment temperature relative to the cooling load (evaporator) temperature presents the need for larger, thus heavier, heat exchangers.

Figure 5 shows the effect of increasing the primary inlet pressure (case 2). It can be seen that increasing $P_{\text{pi}}$ four times its base value caused a slight increase in the overall SMR. Increasing the primary pressure increases the radiator pressure and thus increases the

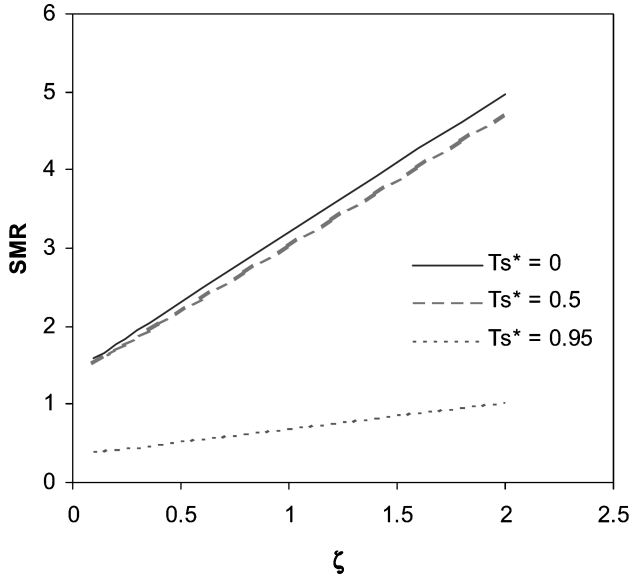


**Fig. 4 Variation of the SMR as a function of the collector parameter $\zeta$ for different normalized sink temperatures $T^*_s$: base case (case 1), $T_{\text{pi}} = -80°\text{C}$, $P_{\text{pi}} = 2$ MPa, $T_{\text{si}} = -175°\text{C}$, $P_{\text{si}} = 0.4$ MPa, $T^*_{\text{col}} = 1.994$, $T^*_{\text{rad}} = 1.303$, and $\xi_T = 1.136$.**

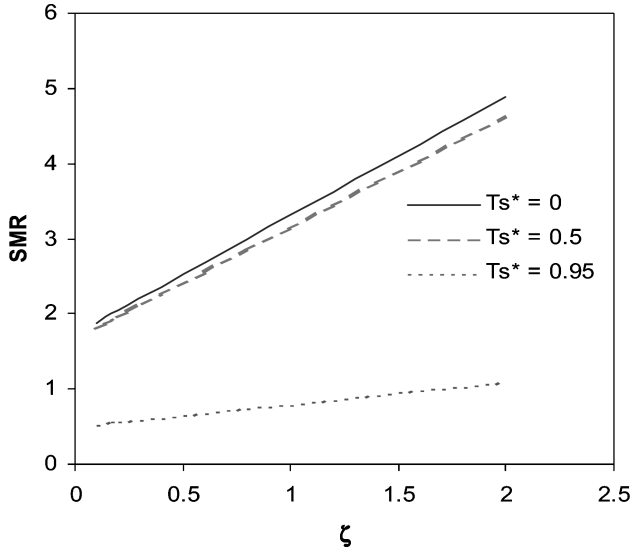


**Fig. 5 Variation of the SMR as a function of the collector parameter $\zeta$ for different normalized sink temperatures $T_s^*$: Effect of $P_{pi}$ is shown by increasing its base value to 8 MPa (case 2), $T_{pi} = -80°C$, $P_{pi} = 8$ MPa, $T_{si} = -175°C$, $P_{si} = 0.4$ MPa, $T_{col}^* = 2.173$, $T_{rad}^* = 1.225$, and $\xi_T = 0.754$.**

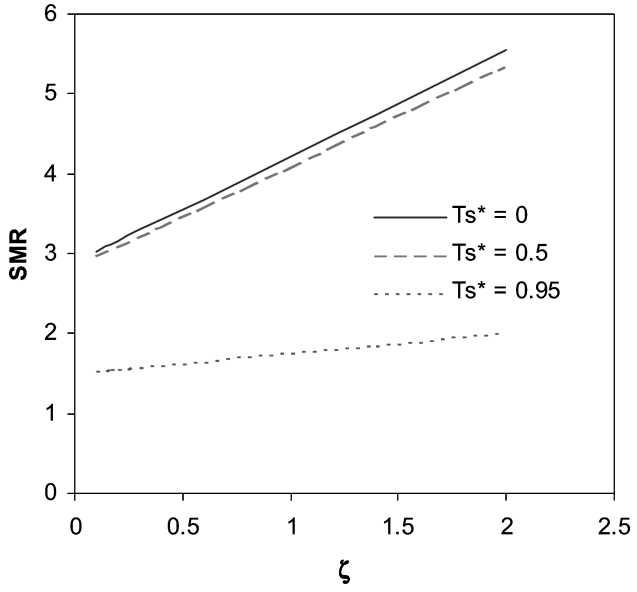


**Fig. 6 Variation of the SMR as a function of the collector parameter $\zeta$ for different normalized sink temperatures $T_s^*$: Effect of $P_{si}$ is shown by increasing its base value to 1.4 MPa (case 3), $T_{pi} = -80°C$, $P_{pi} = 2$ MPa, $T_{si} = -110°C$, $P_{si} = 1.4$ MPa, $T_{col}^* = 1.191$, $T_{rad}^* = 1.06$, and $\xi_T = 0.948$.**

temperature of the saturated part of the working fluid going through the radiator. However, because most of the radiator flow is in the superheated region increasing the primary inlet pressure at a constant temperature decreases the enthalpy of the primary flow. This, in turn, causes a decrease in the temperature of the superheated flow going through the radiator, causing an increase in the overall system mass ratio.

Figure 6 demonstrates that increasing the secondary pressure [low pressure in the refrigeration loop (case 3)] causes an upward shift for the family of curves, indicating an increase in the SMR. The increase in the secondary pressures naturally causes an increase in the evaporator temperature, and thus requires a larger and thus heavier evaporator.

Figure 7 displays the effect of increasing the primary inlet temperature (case 4), causing a significant decrease in the overall SMR, even below one under certain conditions, which clearly shows an

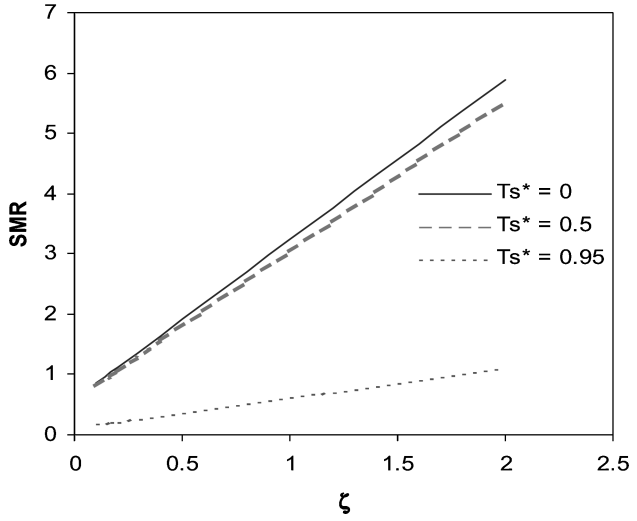


**Fig. 7 Variation of the SMR as a function of the collector parameter $\zeta$ for different normalized sink temperatures $T_s^*$: Effect of $T_{pi}$ is shown by increasing its base value to 40°C (case 4), $T_{pi} = 40°C$, $P_{pi} = 2$ MPa, $T_{si} = -175°C$, $P_{si} = 0.4$ MPa, $T_{col}^* = 3.214$, $T_{rad}^* = 1.709$, and $\xi_T = 1.320$.**

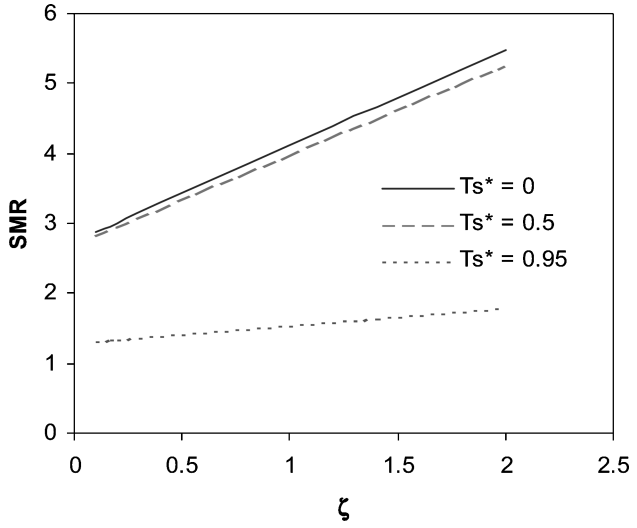


**Fig. 8 Variation of the SMR as a function of the collector parameter $\zeta$ for different normalized sink temperatures $T_s^*$: Effect of $T_{si}$ is shown by increasing its case 4 value to −20°C (case 5), $T_{pi} = 40°C$, $P_{pi} = 2$ MPa, $T_{si} = -20°C$, $P_{si} = 0.4$ MPa, $T_{col}^* = 1.246$, $T_{rad}^* = 1.077$, and $\xi_T = 0.957$.**

apparent advantage of active systems. Increasing the primary inlet temperature yields a higher radiator temperature and thus lowers the size and weight requirements of the radiator heat exchanger.

Figure 8 shows the effect of increasing the value of the secondary inlet temperature (case 5) from its value of case 4 [compare case 5 to case 4, not the base case (case 1)]. Increasing the evaporator temperature (secondary inlet temperature) causes a significant increase in the overall SMR. This effect is attributed to the fact that decreasing the evaporator temperature decreases the cooling capacity, thus increasing the size and weight requirements for the evaporator heat exchanger.

Figures 9 and 10 demonstrate that decreasing the entrainment ratio $\phi$ has an adverse effect on the SMR, whereas increasing it plays a significant role in decreasing the overall SMR. In explaining the variation of the SMR with the entrainment ratio, several competing effects have to be considered. First, increasing the entrainment ratio lowers the compression ratio across the jet pump, causing a decrease in the radiator pressure, and thus lowering the temperature of the saturated part of the radiator flow, which has an adverse effect on the SMR. Second, increasing the entrainment ratio means decreasing

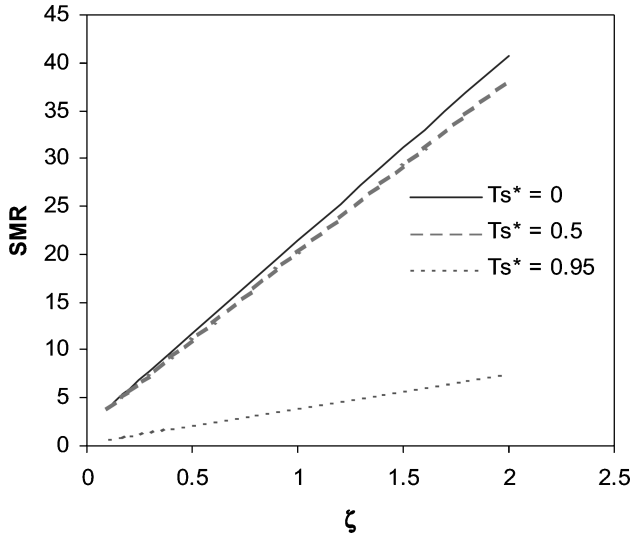


**Fig. 9 Variation of the SMR as a function of the collector parameter $\zeta$ for different normalized sink temperatures $T_s^*$: Effect of $\phi$ is shown by decreasing its base value to 0.2 (case 6), $T_{pi} = -80°C$, $P_{pi} = 2$ MPa, $T_{si} = -175°C$, $P_{si} = 0.4$ MPa, $T^*_{col} = 1.981$, $T^*_{rad} = 1.799$, and $\xi_T = 1.040$.**

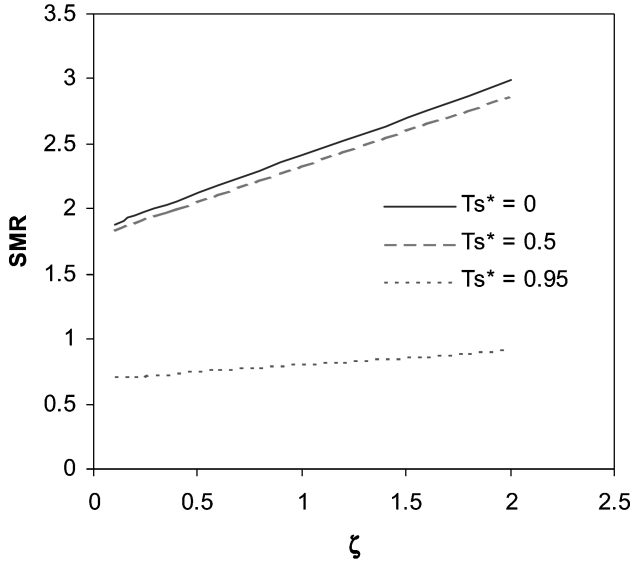


**Fig. 10 Variation of the SMR as a function of the collector parameter $\zeta$ for different normalized sink temperatures $T_s^*$: Effect of $\phi$ is shown by increasing its base value to 6 (case 7), $T_{pi} = -80°C$, $P_{pi} = 2$ MPa, $T_{si} = -175°C$, $P_{si} = 0.4$ MPa, $T^*_{col} = 1.996$, $T^*_{rad} = 1.122$, and $\xi_T = 1.106$.**

the mass flow rate in the refrigeration cycle, and this causes an increase in the evaporator size adding to the overall SMR. However, increasing the entrainment ratio means having higher flow rate in the power cycle, which decreases the required size of the collector, and thus lowers the overall SMR. The net result of the three competing effects decides the behavior of the SMR with respect to the entrainment ratio.

In all of the cases 1–7, the primary and secondary inlet states were in superheated or supercritical states. Figure 11 (case 8) demonstrates the effect of having a liquid–vapor mixture ($x = 0.5$) at the secondary inlet. Case 8 (Fig. 11) should be compared with case 3 (Fig. 6). It is apparent that going from a supercritical state to a mixed state at the secondary inlet had a significant adverse effect on the overall SMR. This is because having a mixed state at the secondary inlet causes a significant decrease in the efficiency of the overall cycle, which is evident by the decrease in the combined efficiency term $\eta$th COP, and the overall percentage Carnot efficiency $\xi_T$. The decrease in efficiency is caused by the decrease in the cooling capacity as well as the amount of heat rejected at the radiator.

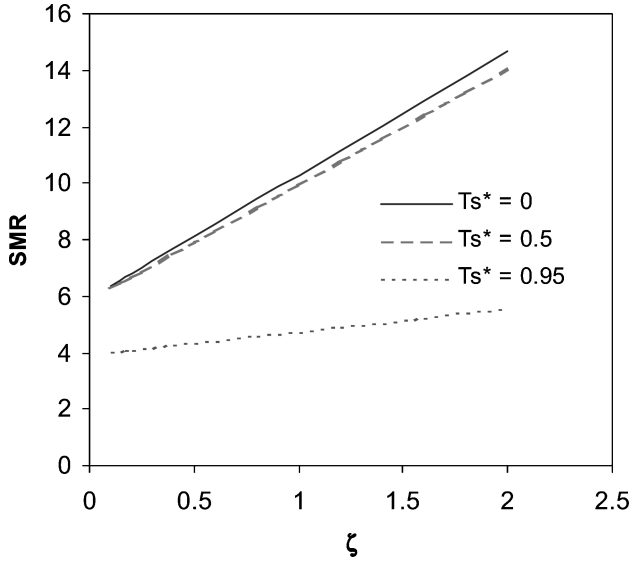


**Fig. 11 Variation of the SMR as a function of the collector parameter $\zeta$ for different normalized sink temperatures $T_s^*$: Effect of having the si state as a liquid vapor mixture (case 8), $T_{pi} = -80°C$, $P_{pi} = 2$ MPa, $T_{si} = -164°C$, $P_{si} = 1.4$ MPa, $T^*_{col} = 1.778$, $T^*_{rad} = 1.031$, and $\xi_T = 0.039$.**

For a particular space application, the environmental and system parameters, which were estimated in order to construct the figures, will be prescribed values. The fluid temperatures of the solar collector and radiator can then be set so as to optimize the mass savings based on Eq. (46). It is observed, for a given value of $T_{col}$, that there exits a value of $T_{rad}$ that will optimize the SMR.

## Conclusions

This paper incorporated the mass-based parameter, system mass ratio (SMR), into the SITMAP cycle analysis to determine the viability of the system analyzed based on weight and economic savings. With the use of this mass parameter, a comparison between active (SITMAP cycle) and passive systems was made to determine conditions under which active systems possess an advantage based on mass savings over their passive counterparts. The conditions were determined by examining the effect of each of the five input parameters to the SITMAP cycle analysis, as well as the parameters for the SMR. The following conclusions can be drawn regarding these dependencies:

1) The overall mass of active systems decreases by minimizing the collector parameter $\zeta$. This parameter is most sensitive to solar-collector technology and the evaporator fluid temperature. Higher collector efficiency and radiator emissivity also directly influence this parameter.

2) The overall mass advantage for active systems increases as the environmental sink temperature is increased, for constant values of all other parameters.

3) The overall SMR is a weak function of the primary inlet pressure. Increasing the primary inlet pressure at a fixed temperature causes a decrease in the temperature of the superheated part of the radiator flow, thus increasing the value of the overall SMR.

4) Increasing the secondary inlet pressure has an adverse effect on the overall mass of active systems.

5) Active systems should be considered, in order to minimize weight, when low evaporator fluid temperatures are desired.

6) Decreasing the weight of piping and turbomachinery will also reduce the value of the system mass ratio and thus reduce the overall system mass.

7) Entrainment ratio variation causes several competing effects regarding the mass of the different components of the cycle. The net result of these competing effects decides the variation of the overall SMR.

8) System mass decreases rapidly with respect to the efficiency $\xi_T$ of both the refrigeration and power subsystems, which in turn

decreases when the secondary inlet state (evaporator exit) is in the two-phase regime.

It follows from the preceding conclusions that, for the configuration and ranges studied, particular active systems can in fact have a significant reduction of mass over more conventional passive systems. Estimation of the values of these parameters can be made during the preliminary design phase of a space mission, allowing an early choice to be made between active and passive thermal management systems. This should simplify and streamline the design process.

## Acknowledgments

This work was partially supported by a grant from NASA. Support from the Department of Mechanical and Aerospace Engineering at the University of Florida is also gratefully acknowledged.

## References

[1]Nord, J. W., Lear, W. E., and Sherif, S. A., "Design Analysis of a Heat-Driven Jet Pumped Cooling System for Space Thermal Management Applications," *Journal of Propulsion and Power*, Vol. 17, No. 3, pp. 566–570.

[2]Freudenberg, K., Lear, W. E., and Sherif, S. A., "Parametric Analysis of a Thermally Actuated Cooling System for Space Applications," *Proceedings of the ASME Advanced Energy Systems Division*, AES-Vol. 40, edited by S. Garimella, M. von Spakovsky, and S. Somasundaram, ASME, New York, 2000, pp. 499–510.

[3]Bredikhin, V. V., Gorbenko, G. A., Nikonov, A. A., and Fairuzov, Y. V., "Mathematical Modeling of Thermo-Circulating Loops with Jet Pumps," *Hydrodynamic Processes in Multi-Phase Working Fluid Energy Plants*, Kharkov Aviation Inst., Kharkov, Ukraine, 1990, pp. 3–10 (in Russian).

[4]Cunningham, R. G., and Dopkin, R. J., "Jet Breakup and the Mixing Throat Lengths for the Liquid Jet Pump," *Journal of Fluids Engineering*, Vol. 96, No. 3, 1974, pp. 216–226.

[5]Cunningham, R. G., "Liquid Jet Pumps for Two-Phase Flows," *Journal of Fluids Engineering*, Vol. 117, No. 2, 1995, pp. 309–316.

[6]Elger, D. F., McLam, E. T., and Taylor, S. J., "A New Way to Represent Jet Pump Performance," *Journal of Fluids Engineering*, Vol. 113, No. 3, 1991, pp. 439–444.

[7]Fabri, J., and Paulon, J., "Theory and Experiments on Air-to-Air Supersonic Ejectors," NACA-TM-1410, Sept. 1958.

[8]Fabri, J., and Siestrunk, R., "Supersonic Air Ejectors," *Advances in Applied Mechanics*, Vol. V, edited by H. L. Dryden, and Th. von Kármán, Academic Press, New York, 1958, pp. 1–33.

[9]Fairuzov, Y. V., and Bredikhin, V. V., "Two Phase Cooling System with a Jet Pump for Spacecraft," *Journal of Thermophysics and Heat Transfer*, Vol. 9, No. 2, 1995, pp. 285–291.

[10]Holladay, J. B., and Hunt, P. L., "Fabrication, Testing, and Analysis of a Flow Boiling Test Facility with Jet Pump and Enhanced Surface Capability," Research Proposal, NASA Marshall Space Flight Center, Thermal and Life Support Division, Huntsville, AL, Jan. 1996.

[11]Holmes, H. R., Geopp, J., and Hewitt, H. W., "Development of the Lockheed Pumped Two Phase Thermal Bus," AIAA Paper 87-1626, June 1987.

[12]Jiao, B., Blais, R. N., and Schmidt, Z., "Efficiency and Pressure Recovery in Hydraulic Jet Pumping of Two-Phase Gas/Liquid Mixtures," *SPE Production Engineering*, Vol. 5, No. 4, 1990, pp. 361–364.

[13]Lear, W. E., Sherif, S. A., Steadham, J. M., Hunt, P. L., and Holladay, J. B., "Design Considerations of Jet Pumps with Supersonic Two-Phase Flow and Shocks," AIAA Paper 99-0461, Jan. 1999.

[14]Marini, M., Massardo, A., Satta, A., and Geraci, M., "Low Area Ratio Aircraft Fuel Jet-Pump Performance with and Without Cavitation," *Journal of Fluids Engineering*, Vol. 114, No. 4, 1992, pp. 626–631.

[15]Neve, R. S., "Diffuser Performance in Two-Phase Jet Pump," *International Journal of Multiphase Flow*, Vol. 17, No. 2, 1991, pp. 267–272.

[16]Sherif, S. A., Lear, W. E., Steadham, J. M., Hunt, P. L., and Holladay, J. B., "Analysis and Modeling of a Two-Phase Jet Pump of a Thermal Management System for Aerospace Applications," *International Journal of Mechanical Sciences*, Vol. 42, No. 2, 2000, pp. 185–198.

[17]Kakabaev, A., and Davletov, A., "A Freon Ejector Solar Cooler," *Geliotekhnika*, Vol. 2, No. 5, 1966, pp. 42–48.

[18]Chen, L. T., "Solar Powered Vapor-Compressive Refrigeration System Using Ejector as the Thermal Compressors," *Proceedings of the National Science Council*, No. 10, Pt. 3, 1977, pp. 115–132.

[19]Lansing, F. L., and Chai, V. W., "Performance of Solar-Powered Vapor-Jet Refrigeration Systems with Selected Working Fluids," DSN Progress Rept. 42-44, Jet Propulsion Lab., Pasadena, CA, 1978, pp. 245–248.

[20]Chai, V. W., and Lansing, F. L., "A Thermodynamic Analysis of a Solar-Powered Jet Refrigeration System," DSN Progress Rept. 41-42, Jet Propulsion Lab., Pasadena, CA, 1977, pp. 209–217.

[21]Abrahamsson, K., Jernqvist, A., and Ally, G., "Thermodynamic Analysis of Absorption Heat Cycles," *Proceedings of the International Absorption Heat Pump Conference*, AES-Vol. 31, American Society of Mechanical Engineers, New York, 1994, pp. 375–383.

[22]Alefeld, G., and Radermacher, R., *Heat Conversion Systems*, CRC Press, Boca Raton, FL, 1994, Chaps. 2, 3, and 4.

[23]Anderson, H., "Assessment of Solar Powered Vapor Jet Air-Conditioning System," *International Solar Energy Congress and Exposition (ISES)*, International Solar Energy Society, Freiburg, Germany, 1975, p. 408.